Astronomy Reports, Vol. 49, No. 2, 2005, pp. 155–166. Translated from Astronomicheskiĭ Zhurnal, Vol. 82, No. 2, 2005, pp. 180–192.

Large-Scale Activity in Solar Eruptive Events of October–November 2003 Observed from SOHO/EIT Data

I. M. Chertok[1] and V. V. Grechnev[2]

[1] *Institute of Terrestrial Magnetism, Ionosphere and Radio Wave Propagation, Troitsk, 142190 Russia*

[2] *Institute of Solar-Terrestrial Physics, Irkutsk, 664033 Russia*

Received June 30, 2004; in final form, July 15, 2004

Abstract—Large-scale solar disturbances associated with powerful flares and coronal mass ejections (CMEs) during two passages of a grand system of three active regions in October–November 2003 are analyzed using data obtained with the SOHO/EIT EUV telescope. Dimmings (transient coronal holes) and, to a lesser extent, coronal waves (traveling emitting fronts) are studied using fixed-difference derotated images, in which a correction for the solar rotation is applied and a single heliogram preceding the event is subtracted from all subsequent heliograms. This method allows us to study difference heliograms in both the 195 Å line (with an interval of 12 min) and the various-temperature channels of 171, 195, 284, and 304 Å (with an interval of six hours). Our analysis shows, in particular, that the disturbances associated with CMEs demonstrated a global character and occupied almost the entire southern half of the disk in virtually all eruptive events during the two solar rotations. At the same time, the northern half of the disk, which had a large coronal hole, was only slightly disturbed. The dominant dimmings were observed on the disk as narrow, long features stretched mainly between three main, well-separated regions of the system and as long structures located along lines of solar latitude in the south polar sector. For repetitive events with intervals between them being not so long, the dominant dimmings demonstrated a clear homology in their forms and locations. During the very powerful event of October 28, one homologous global set of dimmings changed to another set. Many dimmings were observed to be identical or very similar in the three coronal channels and the transition-region line. It follows from the analysis that rapidly recovering global structures in the corona and transition region were involved in the eruption of running CMEs and the corresponding reconstruction of the large-scale magnetic fields.

1. INTRODUCTION

For the decay phase of the 11-year cycle, the solar activity in October–November 2003 was unprecedentedly high. A series of eleven powerful flares from X1 to X28 was recorded by the GOES satellites over fifteen days during the first passage of a system of three large active regions over the solar disk. Over two solar rotations, the white light SOHO/LASCO coronagraph detected dozens of large coronal mass ejections (CMEs), including sixteen halo CMEs with emission observed around all or nearly all of the occulting disk [1]. These eruptive events were accompanied by extreme interplanetary disturbances; a number of proton flux enhancements, in one of which the >10 MeV intensity reached 29 500 $\mathrm{cm}^{-2}\ \mathrm{s}^{-1}\ \mathrm{sr}^{-1}$ near the Earth; geomagnetic storms with $D_{\mathrm{st}} \approx -401$ and -465 nT during the first and second rotations, respectively; deep Forbush decreases in the Galactic cosmic rays; and other associated phenomena (see the Preliminary Report and Forecast of Solar Geophysical Data at http://www.sel.noaa.gov/weekly.html and Solar-Geophysical Data at http://sgd.ngdc.noaa.gov/sgd/jsp/solarindex.jsp, as well as [2]).

This activity is of considerable interest for a variety of studies. The present work is devoted to the analysis of manifestations of solar activity on spatial scales comparable to the solar radius or even the diameter of the visible disk, mainly using data from the SOHO/EIT EUV telescope [3]. In particular, we analyze dimmings and, to a lesser extent, coronal waves associated with CMEs. Recall that dimmings, or transient coronal holes [4–13], are regions of reduced soft X-ray and EUV intensity with lifetimes varying from several hours to a day. These regions are formed after CMEs in the vicinity of eruption centers, for example, on the periphery of pre-eruptive sigmoidal structures, and can cover a significant part of the solar disk. Analysis of Yohkoh/SXT [14] and SOHO/EIT heliograms indicates provides a reason for interpretation of dimmings mainly as a result of complete or partial opening of coronal magnetic fields within these structures in the course of a CME pro-

1063-7729/05/4902-0155$26.00

cess, resulting in evacuation of material and a corresponding decrease of the emission intensity.

Coronal waves are emitting fronts observed ahead of developing dimmings, and can propagate with velocities of several hundred km/s [6, 15–21]. Such a wave is considered as an MHD disturbance or a shock wave, being a coronal analog for the chromospheric Moreton wave observed in Hα [22], or the result of plasma compression at the propagating boundary of a dimming, i.e., at the boundary of the region of open magnetic-field lines [23, 24].

Data and the method of their analysis are addressed in Section 2. Characteristics of large-scale activity are demonstrated in Section 3 for several major events occurred during the first and second passages of the activity complex. The results are discussed in Section 4.

2. DATA AND THE METHOD OF THEIR ANALYSIS

SOHO/EIT observations were performed routinely during the period under study. Heliograms of 1024×1024 pixels with a pixel size of $2.6''$ and a field of view of $45' \times 45'$ were recorded each 12 min in the priority 195 Å EIT channel, which is sensitive to coronal plasma with temperatures of $T_e \approx 1.5$ MK. Four times per day (near 01^h, 07^h, 13^h, and 19^h UT), heliograms were also recorded in two other coronal channels of 171 and 284 Å ($T_e \approx 1.2$ and 2.0 MK, respectively) and in 304 Å channel, which observes the HeII transition-region line ($T_e \approx 0.02$–0.08 MK) [3, 25]. The corresponding FITS files are available at http://umbra.nascom.nasa.gov/eit/eit-catalog.html.

Similarly to [26–28], we use finite-difference derotated images formed in two steps for our analysis. In the first step, the solar rotation is compensated for all heliograms observed during an event using the "rotation" to the time of a pre-selected background heliogram recorded before the event. The derotation was applied to the visible hemisphere by rotating a spherical surface at a heliocentric distance of $r \approx 1R_\odot$. In the second step, the background image was subtracted from all the subsequent derotated heliograms. Such difference images show real changes in the brightness, location, and structure of sources observed during the events. In these images, dimmings appear as dark features of decreased brightness, and a coronal wave appears as a narrow emitting front propagating from the eruption center. As an auxiliary representation, we also use running-difference images formed by subtracting each previous heliogram from the current one. Such images emphasize changes between two running heliograms, but they contain artifacts produced in formation of these images.

To distinguish dimmings and coronal waves from other structures, we constructed the difference images with a limited range of intensities, so that the brightest sources, in particular, those emitting during flares and in post-eruptive phases, usually become saturated.

The derotation method enables us to use the heliograms with six- and twelve-hour intervals to construct and analyze difference images at 195 Å and in all four EIT channels (171, 195, 284, and 304 Å) corresponding to various temperatures [27].

We analyze in this paper both powerful X-ray flares and other major eruptive events that included large CMEs and were accompanied by considerable structural changes on the visible disk. The required information and detailed data on 34 such events (22 and 12 events during the first and second rotations of the active regions, respectively) are presented at the Web-site http://helios.izmiran.troitsk.ru/lars/Chertok/0310_11/index.html. The Web site is arranged as a table containing the date, time, importance, time profiles of soft X-ray emission, and coordinates for each flare. The Web site also contains JAVASCRIPT movies of SOHO/LASCO data along with movies of original (non-subtracted) SOHO/EIT 195 Å images, fixed-difference images, and running-difference images produced from SOHO/EIT 195 Å data as well. In addition, difference images in the 171, 195, 284, and 304 Å channels, as well as Hα movies, are presented for many events. There are summary pictures for groups of events illustrating running CMEs and related large-scale activities on the disk, as well as associated space-weather disturbances in the form of proton-flux enhancements, geomagnetic storms, and Forbush decreases of the Galactic cosmic rays.

3. ANALYSIS OF ERUPTIVE EVENTS

Figure 1 presents a number of heliograms for October 28 illustrating the general situation on the disk. The SOHO/MDI continuum (Fig. 1a) and magnetogram (Fig. 1b) images show that three large active regions dominated on the disk: the western active region AR 484 (Carrington longitude $L = 354$), located slightly to the north from the solar equator at latitude N04, and AR 486 and AR 488, located $60°$–$70°$ to the east ($L = 283$ and 291) at latitudes S15 and N08, respectively.

The southern active region AR 486 had the largest area and most complex structure, and was most active in flare production. The flares with the most

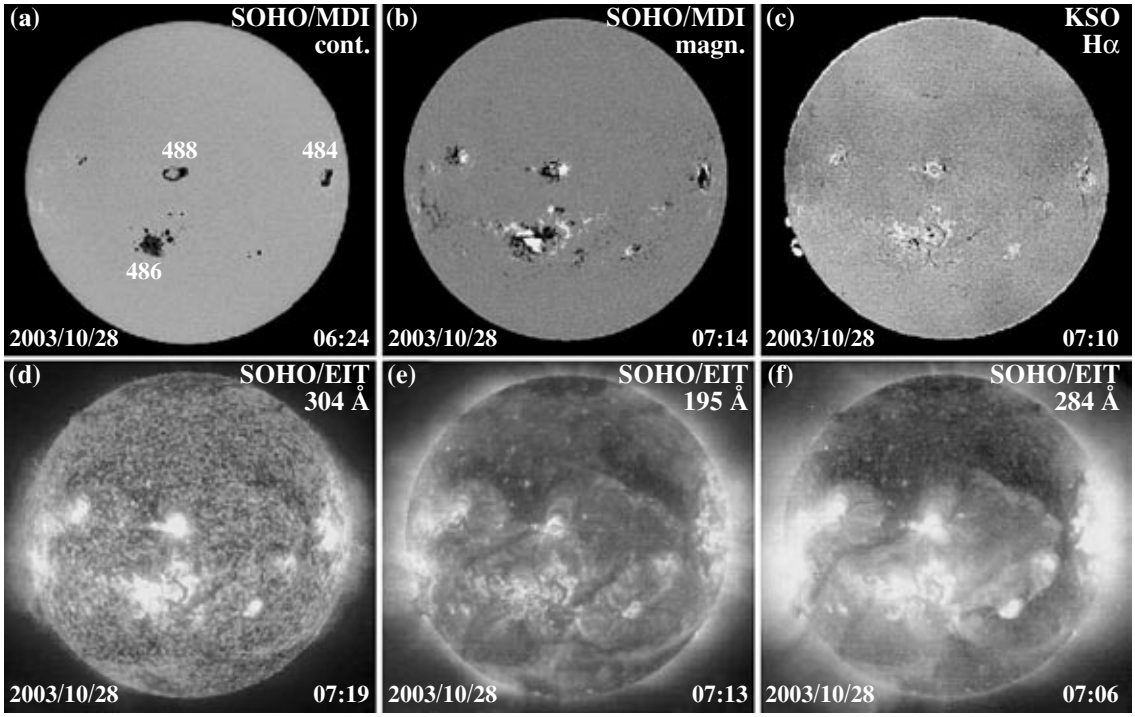

Fig. 1. Images illustrating the situation preceding the event of October 28, 2003. (a) Solar disk in white light; (b) SOHO/MDI magnetogram; (c) KSO Hα heliogram; (d) 304 Å; (e) 195 Å; and (f) 284 Å SOHO/EIT EUV heliograms. The UT is indicated at the bottom right.

powerful X-ray fluxes occurred just in this region. We shall see below that other regions located near and between the three indicated above participated in the events considered, as well as two distant regions located near the eastern limb on October 28. Despite the fact that these regions were well separated in longitude and located on opposite sides of the equator, they were connected to each other by large-scale magnetic fields and constituted one huge activity complex. The Hα heliogram (Fig. 1c) shows dark filaments mainly in and near the active regions, while there were no large filaments in the remainder of the disk.

The SOHO/EIT heliograms in the 304 Å transition-region line (Fig. 1d) and the 195 Å (Fig. 1e) and 284 Å (Fig. 1f) coronal channels also indicate a concentration of active regions in the southern hemisphere and in the near-equatorial zone of the northern hemisphere. According to the high-temperature 284 Å image (Fig. 1f), the dominant visible portion of the northern hemisphere situated to the east of the meridian of AR 484 was occupied by a large coronal hole with numerous coronal bright points and other emitting patches. Narrow extended emitting structures interchanged with sites of decreased EUV emission can be seen at 195 Å in the visible part of the southern hemisphere (Fig. 1e), especially in the polar sector.

3.1. Events during the First Rotation

Figure 2 presents SOHO/EIT difference images at 195 Å illustrating the advanced phases of large-scale disturbances for the twelve most significant eruptive events during the first rotation of the active complex. One of the first events of this type occurred in AR 484 (coordinates N08 E58) on October 19, when the other two large active regions were behind the eastern limb. This event included a 1N/X1.1 flare with its maximum at ~16:50 UT and a partial-halo CME with looplike structures mainly located above the northeastern limb. The difference movies presented at the web site referenced in Section 2 show large-scale disturbances in the form of shallow propagating dimmings and a weak coronal wave occupying almost the entire eastern half of the disk in the interval 16:43–17:22 UT. These disturbances were also observed above the eastern limb. The deepest (darkest) dimmings formed around the bright posteruptive arcade 4 and existed for several hours (Fig. 2a). In addition to the northern dimming 4–1, there was a southern transequatorial dimming 4–2 in the meridional direction. Toward the west,

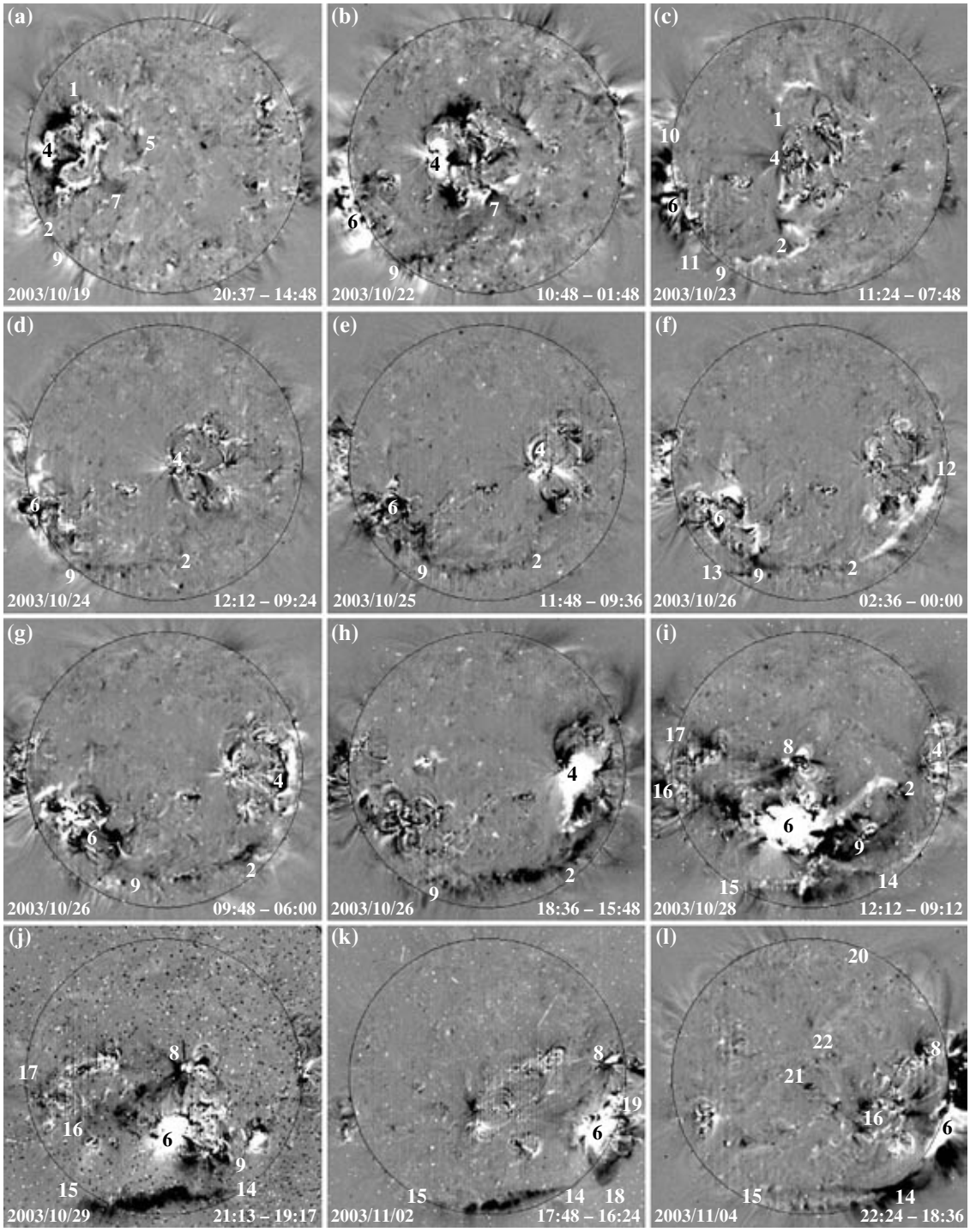

Fig. 2. Derotated SOHO/EIT fixed-difference heliograms at 195 Å showing large-scale disturbances, in particular, dimmings (dark structures), in eruptive events during the first rotation, which occurred between October 19 and November 4, 2003. The date for each event and the UTs for the studied and subtracted images are indicated at the bottom.

the dimming branches went around another large brightening to the points 5 and 7. The narrow dimming structure 7–9 extending toward the southeastern limb was already visible then; this structure played an important role in subsequent events.

A similar dimming structure arose after several eruptive events in AR 484 (N04 E24) on October 22 during the first twelve hours and in AR 496 (S21 $E >$ 90) as it rose from behind the eastern limb. An M1.7 flare at 08:30 UT and a large CME above the north-

ern, southern, and western sectors of the limb were most significant among these events. The compact central (4) and extended southeastern near-limb (6) posteruptive arcades are clearly visible in the difference image of 10:48 UT (Fig. 2b) relative to the background heliogram for 01:48 UT. The main dimmings are observed to the north, south and west of the first arcade corresponding to the CME. A narrow dimming channel 7–9 extending from the intersection of the southwestern brightening and the dimming branch directed toward the southeastern limb becomes clearly visible in this event. Among the other disturbances, this structure was also manifest after the first significant flare detected in AR 486 on October 22 (20:07 UT, M9.9, S21 E90), which was associated with a large CME.

Another powerful near-limb event including a 1B/X5.4 flare and an asymmetric, looplike CME occurred above AR 486 (S12 E88) on October 23 after 08:24 UT (Fig. 2c). This event was first accompanied by a coronal wave propagating along the eastern limb and then by a clear dimming and extended posteruptive arcade located above the large segment of the southeastern limb 10–6–11. Disturbances and various manifestations of activity also occupied the entire southeastern quadrant and the vicinity of AR 484, which was already at the center of the disk. We can see here a narrow meridional dimming 1–4–2 with a branch directed toward the southeastern limb 9 along the same structure that is clearly visible in Fig. 2b. This structure was also displayed by the broken emitting chain 9–2–4 adjacent to the dimming. There were several collimated jets and dimmings directed along the line 4–10, from the center of AR 484 toward the east. The major portion of the northeastern quadrant occupied by the coronal hole was free of significant disturbances, while the northwestern sector of the disk contained a number of dimmings and emitting elements.

Following another near-limb 1N/X1.1 flare on October 23 (20:04 UT, S17 E84) and a second CME, there was similar sympathetic activity in two well-separated regions with similar large-scale disturbances between them.

The events of October 24, when moderate C5.7 and M7.6 X-ray flares and eruptive phenomena occurred alternately in AR 484 and AR 486, clearly show that the southeastern structure indicated above represents a connection between these two regions. In particular, the EIT heliogram in Fig. 2d shows this structure as the narrow dimming 4–2–9–6 containing a segment elongated in latitude in the southeastern high-latitude sector of the disk.

The connection between AR 484 and AR 486 shown by the structure indicated above became even clearer after the eruptive events of October 25, when M1.2–M1.7 flares and a looplike CME were observed during ~05–11 UT in both the western and eastern regions. Figure 2e shows that the deepest and longest dimming, 4–2–9–6, is also well pronounced in this event and appears as a narrow arc with a length comparable to the disk diameter and with its bulge facing the high latitudes of the southern hemisphere. The distant AR 484 and AR 486 are also connected by the weaker, straight, fragmented dimming 4–6. Several additional dimmings extend from the eastern region toward the south and east.

The events of October 26 started with the eruption of a filament located to the south of AR 484. The erupted filament was clearly visible during 00:36–01:25 UT, in the form of a large loop rising above the southwestern limb in the 195 Å EIT movies, which becomes a structured CME in the LASCO coronograph data. The extended posteruptive arcade 2–12 originated at the location of the filament immediately after the eruption (Fig. 2f). It is important that this arcade was an extension of the same arc-shaped dimming 2–9–6 directed toward AR 486, which displayed appreciable activity similar to that of AR 484 during and after the eruption of the filament. The narrow dimming branch 9–13 reached the southeastern limb.

That same day, October 26, there were two more eruptive events with flares with the same classes (X1.2) and X-ray durations and with powerful halo CMEs. The first flare, with optical class 3B, occurred in the eastern active region AR 486 (S15 E44) at ~06:54 UT. However, considerable activity was observed at the same time in the western region AR 484 as well, while the extended arc-shaped southern dimming 6–9–2–4 was developing between these two regions as before (Fig 2g). The corresponding movies show the coronal wave propagating from the center of the eruption to the edge of the northeastern quadrant of the disk.

The second flare of October 26, of optical class 1N, occurred in the western region AR 484 (N02 W38) at ~18:19 UT. During this event, the dimming arc 4–2–9 became clearer and broader, in particular due to numerous dark elements directed toward high latitudes in the southern hemisphere (Fig. 2h). AR 484 displayed the bright posteruptive arcade 4. This time, significant disturbances and large-scale dimmings were also detected to the west and north of the arcade. As a whole, these structures occupied large near-limb and over-limb zones extending from the eastern limb through the southern polar sector and from the western limb toward the northern pole. At the same time, the northern part of the central zone remained almost quiet. This event was the first that was accompanied by a strong proton-flux enhancement near the Earth and "snow" in the EIT and LASCO images, due to

the impacts of energetic particles on the detectors of these instruments.

On October 27, the largest flares had classes of 2F/M2.7 and SF/M5.0, and occurred in the western and eastern regions AR 484 and AR 486, respectively, separated by less than 1 h (at 08:33 UT and 09:27 UT).

The most prominent global disturbances taking the form of large-scale dimmings and a coronal wave occurred on October 28 after 11:10 UT. These were associated with an extremely powerful flare in AR 486, which was located in the central zone of the disk at that time (S16 E08) and had an optical class of 4B and an X-ray flux exceeding X17.2—the limiting level for the GOES detectors. One of the fastest CMEs (2125 km/s in the plane of the sky), which had the form of a complete halo with uniform ring-shaped emission around the entire occulting disk, was observed during this event. It was responsible for the strongest geomagnetic storm during the first rotation. Significant flare brightenings started at approximately 10:00 UT in AR 486, also encompassing AR 488, which was located at a neighboring longitude but somewhat to the north from the solar equator (N08 E03), thus preceding the main event (see the Web-site, Fig. 1, and Fig. 2i). The brightenings in these regions were accompanied by a transequatorial dimming between them and by disturbances propagating toward the east. The coronal wave and comparatively shallow traveling dimmings, which occupied the entire northern hemisphere despite the coronal hole observed there, followed the main energy release, which occurred in AR 486 at 11:10 UT. The deepest and longest dimmings occurred throughout the southern hemisphere (Fig. 2i). The southern dimming that earlier connected AR 484 and AR 486 was transformed into the long dimming structure 6–9–2–4, which was appreciably broadened near the bright posteruptive arcade and shifted somewhat toward the north from its previous position. Another narrow dimming 6–14 originating from the eruption center reached the southern subpolar zone, where it was transformed into the high-latitude east–west dimming 14–15 which would dominate in subsequent events. During 11:24–12:12 UT, the luminous material 6–2, shown in Fig. 2i as a structure reaching the central portion of the dimming 6–9–2–4, was ejected from the arcade toward the northwest.

The northwestern and northeastern ends of the posteruptive arcade 6 were connected with the northern near-equatorial region AR 488 by transequatorial dimmings. Global disturbances in the southern hemisphere were accompanied by the two dimming strips 6–16 and 8–17 extending from both central regions toward the eastern limb.

Another powerful event with a 2B/X10 flare and very similar symmetric halo CME occurred in AR 486 (S15 W02) on the following day, October 29, at approximately 20:49 UT. In this case (Fig. 2j), the southern polar dimming 14–15 formed during the previous event dominates in the heliograms covered by "snow" due to the intense flux of accelerated particles. The western dimming adjacent to the bright posteruptive arcade is visible only in the segment 6–9. Its eastern portion is connected with the western sector of the southern polar dimming 14–15 by several meridional elements. A chain of fragmented dimmings extends along 6–16, to the east of the posteruptive arcade. The connection between the two central active regions AR 486 and AR 488 is indicated by the transequatorial dimming 6–8. The diagonal dimming 8–16 originates from the northern region, as well as the fragmented dimming structure 8–17 extending to the eastern limb.

The next three days were comparatively quiet: there were only two marked eruptive events related to flares in AR 486 on October 31 (17:20 UT, SF/C5.3, S20 W28) and November 1 (22:38 UT, 1N/M3.2, S12 W50). Appreciable, though not such large-scale, CMEs and dimmings were observed to the west of AR 486 in both cases.

The activity recommenced in the southwestern region AR 486 (S14 W56) on November 2 at ~17:25 UT, taking the form of a 2B/X8.3 flare and large CME above the western limb with an angular size of ~180°. Similarly to the event of October 29 (Fig. 2j), the southern polar dimming 14–15 along with the posteruptive arcade 6 dominated in the difference EUV heliograms (Fig. 2k). The limb dimming 18–19 was located directly above the arcade. In addition, disturbances occupied the vicinity of the northern near-equatorial region AR 488 and the entire disk sector between this region and the central meridian. To the north of AR 488, traveling disturbances similar to a coronal wave were observed near the flare maximum.

The events of November 3 were associated with activity in the northern, near-equatorial region AR 488 (N09 W80), where two flares of classes 2B/X2.7 and 2F/X3.9 occurred at 01:30 and 09:55 UT, respectively. The corresponding CMEs were observed mainly above the northwestern limb. In both cases, the EUV heliograms and CME images displayed so much snow due to energetic particles that large-scale disturbances were almost indiscernible.

An extremely powerful X-ray flare (whose class exceeded the limiting level X17.2, reaching an estimated maximum of X28) occurred on November 4 in AR 486 at ~19:53 UT, when it was situated near the

southwestern limb (S19 W83). During this event, a clear dimming was observed around the pronounced posteruptive arcade 6 above the entire southwestern limb (Fig. 2l). The looplike dimming 8–20 originating from AR 488 was observed above the northwestern limb. The angular size of the large CME corresponds to the range of position angles for near-limb dimmings. The southern subpolar dimming 14–15, split here into two extended strips, is again clearly visible. Its western end 14 approaches the main dimming above the southwestern limb, forming a single global dimming structure. Similar to the event of November 2 (Fig. 2k), disturbances occupy the entire southwestern quadrant, where two dimming channels 16–21 and 16–22 reaching the central zone of the disk can be seen.

So far we have considered the SOHO/EIT images at 195 Å. The derotation technique also enables us to construct and analyze difference heliograms in the remaining channels at 171, 284, and 304 Å using the data taken at six-hour intervals. With this interval between heliograms, we cannot assume that all events are isolated. In addition, the heliograms became full of snow due to accelerated particles one to two hours after the powerful western events that began from October 28. Allowing for these limitations, the EIT website indicated above does not present simultaneous difference images in the four lines for every event of this series.

Figure 3 shows such heliograms for two events during the first rotation. For the first of these, which occurred in the evening of October 26 (see Figs. 3a–3d, and also Fig. 2h), the difference heliograms in the three coronal channels (Figs. 3b–3d) demonstrate dimming structures that are similar in form and location; namely, the extended southern arc 4–2–9 noted above and the dimming 4–23 located to the north of the posteruptive arcade. In the transition-region line (Fig. 3a), the dimming arc displays only faint fragments, while the northern dimming shows only a portion adjacent to the eruptive center 4. The northern base 24 of the large-scale loop above the northwestern limb is a dimming in the coronal lines corresponding to low (171 Å) and moderate (195 Å) temperatures, while its southern base 25 is visible in the coronal lines corresponding to moderate and high (284 Å) temperatures. The dominant portion of the northwestern over-limb loop is observed at 284 Å. Distinct dimmings are also visible above the southwestern limb in the same channel.

Figures 3e–3h show difference heliograms for the second event on November 4 (see Fig. 4l) in the four channels for the time interval from 19^h UT on November 4 to 01^h UT on November 5. The heliograms at 171 Å (Fig. 3f) and 195 Å (Fig. 3g) display the single dimming 14–15 extended in latitude in the southern polar sector. Only the western part of this dimming is visible in the 304 Å transition-region line (Fig. 3e), while the dimming is almost invisible in the 284 Å coronal high-temperature line (Fig. 3h). However, here, and to a lesser extent at 195 Å, a large dimming is clearly visible around the posteruptive arcade 6 above the southwestern limb. The southern fragment of this dimming is also visible at 304 Å (Fig. 3e). As a whole, the over-limb dimming and the dimming extended in latitude on the disk form a single global dimming structure.

3.2. Events during the Second Rotation

The considerable activity appears to have continued when the active regions were in the invisible hemisphere, as is demonstrated by the presence of numerous large CMEs, including five halo CMEs (without corresponding effects on the visible disk), detected by the LASCO coronograph between November 6–12. The leading northern near-equatorial region AR 501 (N03, $L = 002$), which was numbered AR 484 in the first rotation, was most active during the first half of the second rotation, from November 13–20. Of the two following regions of the first rotation (AR 488 and AR 486), the northern region AR 507 (N10, $L = 295$) manifested itself on November 20, while the southern region AR 508 (S20, $L = 286$), which was near the western limb, gave rise to large events on November 27 and December 2. In general, the events observed during the second passage of the active regions were not as prominent as those during the first rotation, in terms of both flares and CMEs and accompanying phenomena in the EUV. This conclusion is supported, in particular, by Fig. 4, which presents the derotated SOHO/EIT difference heliograms at 195 Å for the developed phase of the largest eruptive events during the second rotation, analogous to Fig. 2.

Two eruptive events occurred on November 13, when the first region (AR 501) reached the eastern limb. The largest event was related to a prolonged M1.4 flare (09:29 UT, N04 E90) and a partial-halo CME containing a bright looplike front above the eastern limb. The angular size of this CME was about 180°, which corresponds to the size of the near-limb zone occupied by disturbances visible in the EUV heliogram (Fig. 4a). Large dimmings and individual emittive structures developed around the extended posteruptive arcade 1 above the limb. On the disk, large-scale disturbances in the form of fragments of a coronal wave and dimmings (for example, 1–2–3 and 1–4) adjacent to the eastern limb were observed within an arc-shaped sector, which reached the central meridian in the southern and northern polar zones.

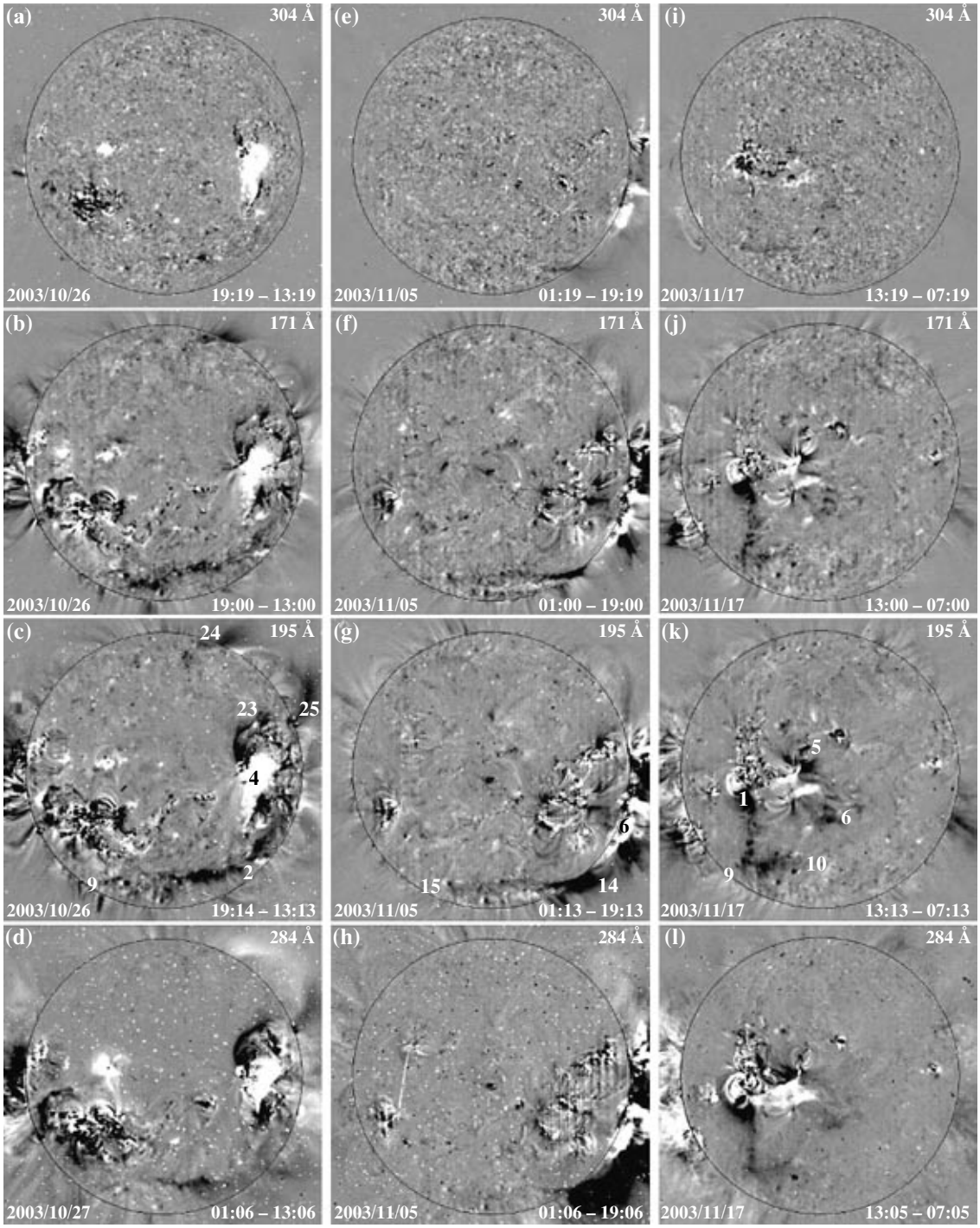

Fig. 3. Derotated SOHO/EIT difference heliograms at intervals of six hours in the four channels at 304, 171, 195, and 204 Å demonstrating dimmings in lines of various temperatures for two events during the first and one event during the second rotations: (a–d) October 28; (e–h) November 4; (i–l) November 17, 2003. Image (d) shows a difference image obtained an interval of twelve hours, since the 284 Å heliogram for October 26 19^h UT is absent.

The next marked event, which was associated with a 1N/M4.2 flare and another southeastern partial-halo CME, also occurred in AR 501 (S01 E33), on November 17 at 09:05 UT. We can see a number of additional luminous strips and arcs surrounded by the dimmings 5 and 6 located to the west of the main flare source 1 in the EUV heliogram (Fig. 4b). The main extended dimming first developed toward the

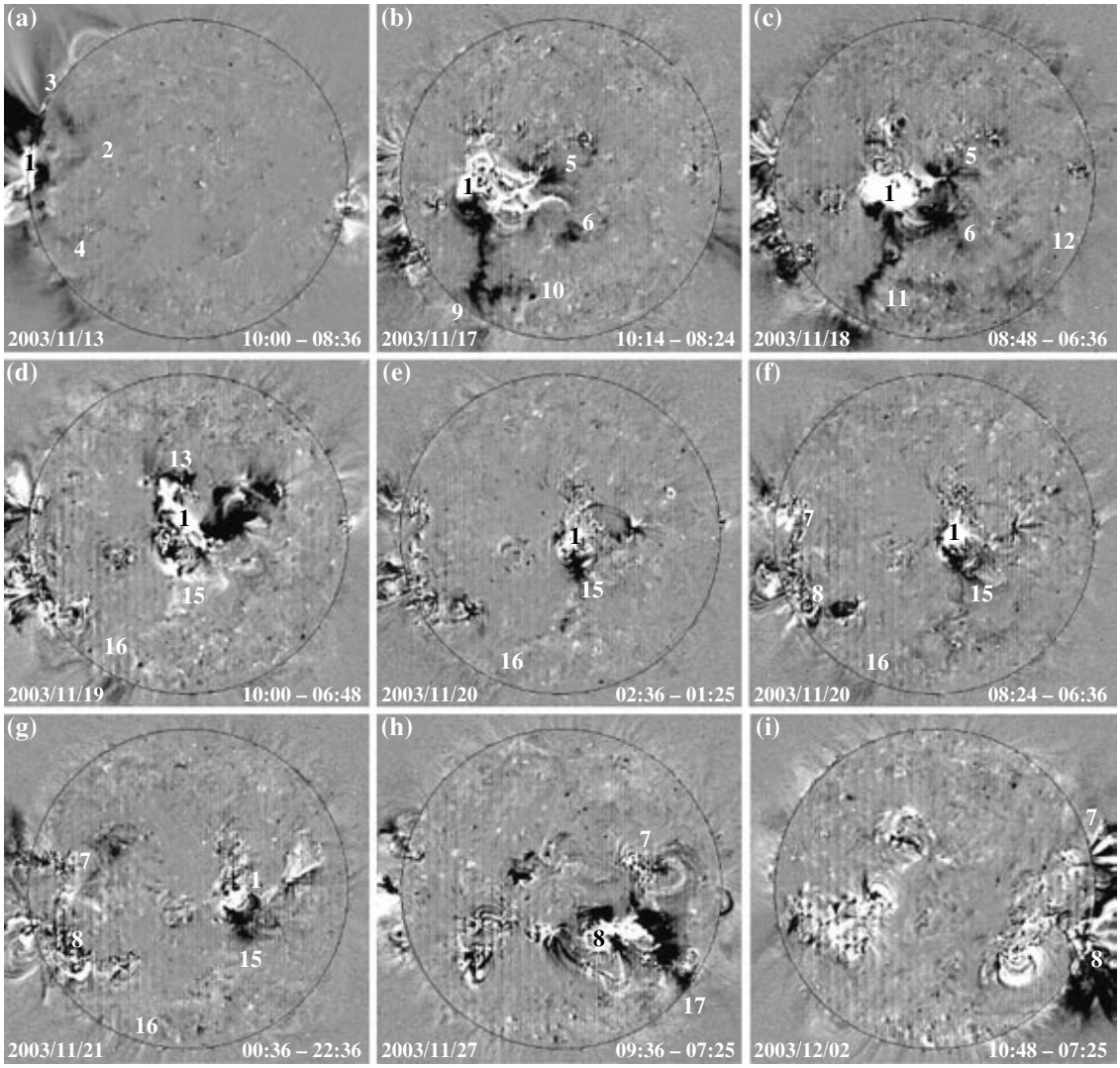

Fig. 4. Derotated SOHO/EIT difference heliograms at 195 Å displaying dimmings in eruptive events during the second rotation, observed between November 13 and December 2, 2003.

south (1–9), then was supplemented with a western branch 9–10. The corresponding movies show comparatively weak disturbances similar to coronal waves in a large zone reaching the southwestern limb. It was the western edge rather than the leading front that was brightest in this CME, probably because the western edge is an extension of the main southern dimming 1–9–10, which ejected most of the material.

The most interest is aroused by a prolonged, class 2N optical flare occurring in AR 501 (N08 E18) on November 18, which was accompanied by two M3.2 and M3.9 X-ray bursts at 07:52 and 08:31 UT, respectively; a third M4.5 X-ray burst whose maximum was observed at 10:11 UT is attributed to activity on the eastern limb. The corresponding CME also had multiple components. First, a comparatively weak CME whose brightest part was its western front, as for the CME of November 17, was observed above the southeastern limb. Then, a much brighter, faster, and larger-scale partial-halo CME developed above the southern and southwestern limb after ~08:40 UT. Despite the moderate magnitude of this flare, this event gave rise to a very strong geomagnetic storm with $D_{st} \approx -465$ nT on November 20. The CME eruption was accompanied by considerable EUV disturbances occupying almost the entire southern hemisphere (Fig. 4c). Similar to the event of November 17, the deep dimmings 5 and 6 occurred in the vicinity of the western part of the eruptive center 1. However, the main extended dimming 1–9 corresponding to the first CME was extended toward the south/southwestern limb as before. A complex set of disturbances, both stationary and traveling from the eruptive center, was observed throughout

the southeastern quadrant during several tens of minutes before the second powerful CME. Some of the fragmented and concentric arc-shaped dimmings formed here (for example 11–12) can be seen in Fig. 4c, while the coronal wave is much more visible in the movie of the running-difference images (see the website). The third large CME observed above the southeastern limb after 09:26 UT can probably be attributed to activity in an adjacent sector of the invisible hemisphere, some manifestations of which can be seen above the limb in the EIT heliograms.

In contrast to the preceding events, a 1F/C8.8 flare occurred on November 19 at 08:17 UT in the northern but not the southern part of AR 501 (N08 E01 in Fig. 4d). Accordingly, the extended posteruptive arcade 1, dimmings 13 and 14 adjacent to the arcade ends, accompanying disturbances, and a comparatively small looplike CME were observed mainly to the north of the solar equator, in the northwestern sector and above the northwestern limb. The southern hemisphere was affected only slightly, via the southeastern structure 15–16, whose position coincides with the main extended southern dimming observed in many events of the first rotation.

The same structure 1–15–16, extending from the eruptive center toward the southeastern limb and probably farther toward the southern region AR 508, which had appeared on the disk, was indicated in the form of comparatively faint, fragmented dimmings in several weak events on November 20–21 (Figs. 4e–4g). The main dimmings in these events were observed in the vicinity of the southern part of the central region AR 501 (N03 W10), where some short X-ray flares with classes between C8.8 and M9.6 occurred, together with small CMEs and weak disturbances in the southwestern sector.

One more substantial event with a C8.6 flare was observed in the northern region AR 507 (N09 E58) on November 20 at 19:29 UT. This event was accompanied by disturbances developing around this region, including transequatorial dimmings located between AR 507 and AR 508.

Two last large events of this series occurred in the southern region AR 508 only in the approach toward the southwestern limb. The first (Fig. 4h) occurred on November 27 at 08:20 UT after a prolonged SF/C9.6 flare (S14 W37) and a southwestern CME that was comparatively small in angular size. The corresponding dimmings formed around the posteruptive arcade 8, extended toward the northern region 7, and ultimately reached the southwestern limb 17.

The last event of December 2 occurred at 09:48 UT (Fig. 4i); this was a limb event (S14 W90) including a C7.2 flare with a prolonged burst of soft X-rays and a large southwestern CME. In this case, the dimmings were mainly observed above the limb, and occupied the same angular sector as the CME, extending from the northern region 7 to the southern polar zone. Against these dimmings, narrow luminous structures emerged from the vicinities of the two limb regions 7 and 8.

We can examine the dimming features of the event of November 17 (Fig. 4b) in various lines using the difference heliograms at intervals of six hours presented in Figs. 3i–3l. The main meridional dimming 1–9 and its western branch 9–10, as well as the dimmings 5 and 6 adjacent to the ribbons of emission near the eruptive center, are manifest in the same way in the three coronal channels at 171, 195, and 284 Å (Figs. 4j–4l). Moreover, comparatively faint analogs of these dimmings (in particular, of the main dimming 1–9–10) can be seen in the 304 Å heliogram (Fig. 4i).

4. DISCUSSION AND CONCLUSIONS

Analysis of SOHO/EIT EUV heliograms using compensation of the solar rotation and formation of fixed-difference derotated images has enabled us to reveal some characteristic features of the large-scale activity in a series of powerful eruptive events in October–November 2003. The main features are the global character of the activity occurring in a single system containing three large sunspot groups, and the homology of the dimmings accompanying the eruptions of numerous halo CMEs.

The global character of the activity was manifested, in particular, by the fact that the disturbances associated with the CMEs in many events occupied appreciable portions of the solar magnetosphere. Some dimmings whose spatial sizes were comparable to the radius or even the diameter of the solar disk occupied almost the entire southern hemisphere, and took the form of extended structures connecting distant active regions, including those located on opposite sides of the solar equator. The southern arc-shaped structure 4–2–9–6 (Fig. 2) was the most significant of such dimmings. These dimmings indicate that there was a magnetic connection between the regions participating in the active system observed. In addition, some events were accompanied by coronal waves, which, in contrast to dimmings, propagated mainly through the northern half of the disk. In general, the entire visible part of the global solar magnetosphere frequently became involved in the eruption of a CME.

The behavior that we call large-scale homology includes prominent dimmings formed in the same magnetic structures with considerable spatial sizes during repeated eruptive events. Homologous dimmings in transequatorial loops associated with flares and CMEs that occurred at the beginning of May

1998 were analyzed in [29]. Homologous large-scale disturbances (dimmings and coronal waves) associated with a single active region in a series of eruptive events at the end of November 2000 were described in [30]. An important feature of the series of events observed during the first rotation of the three active regions considered here is the much larger spatial size of the dimmings and their reconstruction from one set of homologous dimmings to another observed on October 28 (see Fig. 2; this reconstruction is also clearly visible in the movie presented at the EIT web site). Whereas the extended dimming arc 4–2–9–6 dominated in a number of events preceding the reconstruction, the southern subpolar dimming 14–15 elongated in latitude clearly dominated in succeeding events. During the second rotation, when the activity was not as powerful, the southern meridional dimmings 1–9 observed on November 17 and 18 (Fig. 4) can probably be considered homologous. The existence of large-scale, homologous dimmings occurring in repeated events indicates, first, that the eruption of running CMEs involves the same structures of the global solar magnetosphere and, second, that these structures have time to recover their EUV luminosity over the ten to fifteen hours between running CMEs.

Our analysis shows that, in many events, the main dimmings appear essentially identical or very similar in the three coronal lines at 171, 195, and 284 Å and the 304 Å transition-region line (compare with [27]). Here, we must take account of the fact that dimmings observed at 304 Å in the immediate vicinity of eruptive centers (active regions) may be due partially to the weakening of the emission in the coronal Si XI line, which is also in the 304 Å channel [3, 25]. A coincidence of dimmings in lines with various excitation temperatures is usually considered as a support of the idea [6, 7, 10] that such dimmings result from the outflow of plasma during a partial or complete opening of the magnetic-field structures occurring in association with CMEs. Direct evidence for an outflow of material from dimmings located near an eruptive center was found in [12] via an analysis of the Doppler shifts of several lines detected with the SOHO/CDS spectrometer [31]. However, in order to conclude that the opening of magnetic-field lines plays a dominant role, we require additional evidence, since the observations (including those discussed here) show that structures subject to dimmings frequently remain visible in emission after the CMEs, although they are much weaker. In addition, it is not entirely clear how the partial or complete opening of the magnetic-field lines in dimmings can be reconciled with the rather rapid recovery of their luminosity in homologous events. Along with coincident dimmings, there are also dimmings that differ in the different coronal lines and transition-region line [27]. This indicates that a weakening of the EUV intensities in some lines combined with the absence of such weakening or even some strengthening in other lines can be initiated by changes in the plasma temperature, for example, due to heating or MHD disturbances associated with CMEs. The formation of dimmings is probably associated with various factors, including deformations of magnetic structures, variations in the flow of chromospheric material into the coronal loops under CMEs, etc., as well as the opening of magnetic-field lines and temperature variations.

The general behavior of the activity in the events of October–November 2003 shows that we observed an unprecedented powerful global burst of activity that demonstrated a simultaneous emergence of three powerful magnetic fluxes from the photosphere and the formation of three large sunspot groups that were well-separated but connected to each other. The evolution of the local and large-scale magnetic fields of this global system gave rise to a series of analogous powerful flares and prominent CMEs, which were accompanied by homologous large-scale disturbances in the solar atmosphere. The causes of such strong fluctuations in the decay phase of the 11-year activity cycle remains unknown.

ACKNOWLEDGMENTS

The authors are grateful to the SOHO/EIT team for the data used. This work was supported by the Russian Foundation for Basic Research (project nos. 03-02-16049 and 03-02-16591), the Russian Ministry for Education and Science (Program for the Support of Leading Scientific Schools of Russia, projects NSh-477.2003.2 and NSh-1445.2003.2), and the program of the Russian Academy of Sciences "Nonstationary Processes in Astronomy."

REFERENCES

1. G. E. Brueckner, R. A. Howard, M. J. Koomen, *et al.*, Solar Phys. **162**, 357 (1995).
2. I. S. Veselovskiĭ *et al.*, Kosmich. Issled. **42**, 453 (2004) [Space Res. **35**, 433 (2004)].
3. J.-P. Delaboudinière, G. E. Artzner, J. Brunaud, *et al.*, Solar Phys. **162**, 291 (1995).
4. A. C. Sterling and H. S. Hudson, Astrophys. J. **491**, L55 (1997).
5. H. S. Hudson and D. F. Webb, in *Coronal Mass Ejections*, Ed. by N. Crooker, J. Joselyn, and J. Feynman, AGU Geophysical Monograph Series, No. 99, 27 (1997).
6. B. J. Thompson, S. P. Plunkett, J. B. Gurman, *et al.*, Geophys. Res. Lett. **25**, 2465 (1998).
7. D. M. Zarro, A. C. Sterling, B. J. Thompson, *et al.*, Astrophys. J. **520**, L139 (1999).

8. D. F. Webb, J. Atmos. Solar-Terr. Phys. **62**, 1415 (2000).
9. A. S. Sterling, J. Atmos. Solar-Terr. Phys. **62**, 1427 (2000).
10. N. Gopalswamy and B. J. Thompson, J. Atmos. Solar-Terr. Phys. **62**, 1458 (2000).
11. H. S. Hudson and E. W. Cliver, J. Geophys. Res. **106**, 25199 (2001).
12. L. K. Harra and A. C. Sterling, Astrophys. J. **561**, L215 (2001).
13. S. W. Kahler and H. S. Hudson, J. Geophys. Res. **106**, 29239 (2001).
14. S. Tsuneta, L. Acton, M. Bruner, *et al.*, Solar Phys. **136**, 37 (1991).
15. B. J. Thompson, J. B. Gurman, W. M. Neupert, *et al.*, Astrophys. J. **517**, L151 (1999).
16. A. Klassen, H. Aurass, G. Mann, *et al.*, Astron. Astrophys. **141**, 357 (2000).
17. B. J. Thompson, B. Reynolds, H. Aurass, *et al.*, Solar Phys. **193**, 161 (2000).
18. A. Warmuth, B. Vršnak, H. Aurass, *et al.*, Astrophys. J. **560**, L105 (2001).
19. D. A. Biesecker, D. C. Myers, B. J. Thompson, *et al.*, Astrophys. J. **569**, 1009 (2002).
20. N. Narukage, H. S. Hudson, T. Morimoto, *et al.*, Astrophys. J. **572**, L109 (2002).
21. J. L. Khan and H. Aurass, Astron. Astrophys. **383**, 1018 (2002).
22. G. E. Moreton and H. E. Ramsey, Publ. Astron. Soc. Pac. **72**, 357 (1960).
23. C. Delannée and G. Aulanier, Solar Phys. **190**, 107 (1999).
24. C. Delannée, Astrophys. J. **545**, 512 (2000).
25. D. Moses, F. Clette, J.-P. Delaboudinière, *et al.*, Solar Phys. **175**, 571 (1997).
26. I. M. Chertok and V. V. Grechnev, Astron. Zh. **80**, 162 (2003) [Astron. Rep. **47**, 139 (2003)].
27. I. M. Chertok and V. V. Grechnev, Astron. Zh. **80**, 1013 (2003) [Astron. Rep. **47**, 934 (2003)].
28. I. M. Chertok and V. V. Grechnev, Solar Phys. (2004, in press).
29. J. I. Khan and H. S. Hudson, Geophys. Res. Lett. **27**, 1083 (2000).
30. I. M. Chertok, V. V. Grechnev, H. S. Hudson, and N. V. Nitta, J. Geophys. Res. **109**, A02112 (2004).
31. R. A. Harrison, E. C. Sawyer, and M. K. Carter, Solar Phys. **162**, 233 (1995).

Translated by V. Badin